Finite Element Approach for Optimizing the Cooling of Metallic Bipolar Plates for Fuel Cell Applications

E. Firat*[1,2], L. Kühnemann[1,2], C. Siegel[1,2], P. Beckhaus[1] and A. Heinzel[1,2]
[1]Zentrum für Brennstoffzellentechnik (ZBT) GmbH, Duisburg
[2]University of Duisburg Essen
*Corresponding author: Zentrum für BrennstoffzellenTechnik (ZBT) GmbH Carl-Benz-Straße 201, D-47057 Duisburg, Germany, e.firat@zbt-duisburg.de

Abstract: Metallic bipolar plates promise several advantages for fuel cell applications. On the other hand, cooling of these plates is a critical task regarding design optimization. The high thermal conductivity of the material and the complex geometry of these plates affect directly the cooling performance. To analyze this phenomenon, a 3D model is set-up and solved using a FEM (finite element method) approach. The obtained cell geometry is imported with the CAD import module and simplified using symmetry conditions. As for the physics, momentum transport is used to describe the fluid flow through the cooling channels. Energy transport takes the heat transfer (cooling) into account. Structural optimization of the metallic bipolar plates is made simultaneously in order to obtain an evenly distributed temperature profile. The effect of different geometries on the temperature distribution is compared regarding the same cell operating point.

Keywords: Fuel cell, metallic bipolar plates, cooling, multiphysics

1. Introduction

Fuel cell systems with metallic bipolar plates are of great interest in research and industry due to several significant advantages such as high mechanical stability, and excellent electrical and thermal conductivity as stated in [1]. Material properties of metallic bipolar plates yield a higher energy density and allow building cheaper fuel cell stacks compared to graphite bipolar plates [2]. The possible energy density is up to 2 [kW/kg], which facilitates compact automotive applications [3]. Graphite compounded bipolar plates have some disadvantages, especially regarding high viscous material properties which restricts manufacturing abilities [3]. Beside all benefits, metallic bipolar plates cause additional challenging points. The high corrosion sensitivity of these plates under (PEM) polymer electrolyte membrane fuel cell operating conditions requires coated surfaces [4]. Moreover, the type of the cooling medium is restricted.

Cooling of PEM fuel cells plays a critical role regarding both the efficiency and the durability of all components. These systems are operated in a narrow temperature range of several degrees. In order to prevent drying out of the membrane and/or excessive thermal stresses, an adequate thermal management is required [5]. It is challenging to remove the generated heat which has almost the same amount as the produced electrical energy. Due to the high thermal conductivity and constructive restrictions the convenient cooling of metallic bipolar plates must be taken into consideration during the design process. For evaluation of the cooling structures, using simulation environments is an effective approach.

In this study, the simulation tool COMSOL Multiphysics® is used to design an appropriate cooling concept. The cooling medium flow and the heat transfer through metallic bipolar plates are simulated in order to analyze the appropriate physical behavior. Selected simulations are performed under different boundary conditions in order to compare and evaluate the effect of parameters (e.g. the velocity of the inlet cooling air) on the cooling of metallic bipolar plates. Simultaneous optimization of the geometry is added to the 3D model. Getting homogenous temperature distribution is the main aim of the design process in order to increase the kinetic rates inside PEM fuel cells and optimize the performance as shown in [6].

2. Use of COMSOL Multiphysics®

2.1 Model Set-up

The metallic bipolar plate under consideration is such structured that it enables air cooling (or cooling via another cooling medium)

on the other side (backside of the plate). This approach saves an additional plate and increases the overall cooling efficiency. As can be seen from Fig.1, both faces of the plate have a channeled structure allowing the two media to flow separately through (or along) both sides of the metallic bipolar plate. Constructive difficulties are solved by using new manufacturing techniques.

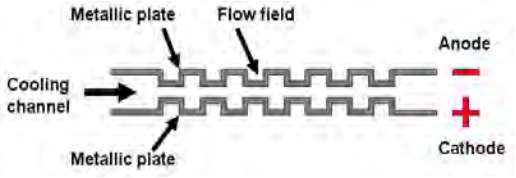

Figure 1. Metallic bipolar plate structured on both sides.

Several methods exist to analyze a cooling process. This can be performed by using:

- heat transfer coefficient on the convection cooled surfaces
- Extending the model to describe the flow and heat transfer

Herein, the first method is chosen since it is powerful and very efficient considering the complexity of the present geometry. Moreover, computational costs are significantly less as explained in [7].

The 3D model geometry is prepared with an advanced CAD tool including all geometric features.

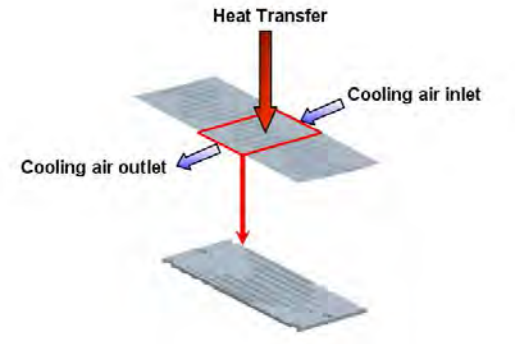

Figure 2. Model geometry of the cooling medium.

The cooling channel, namely the negative form, is separately modeled with the aim of simulations. Symmetry conditions lead to a significant reduction of the 3D model geometry. Finally, it is imported in STEP format with the help of CAD import module of COMSOL Multiphysics®. Repairing of the geometry is performed if necessary.

The final model geometry as well as the considered constraints are shown in Fig.2. The air inlet and outlet for the cooling medium can also be seen in this figure.

2.2 Subdomain Equations

Incompressible Navier-Stokes and general heat transfer application modes are used to describe cooling medium flow through the channels. The steady state equations are used in their non-conservative form. The coupling of both application modes is obtained by using the velocity vector of Eq.(1) in the convective heat flux term of Eq.(2).

$$\rho(\underline{u}\cdot\nabla)\underline{u}+\nabla p=\nabla\cdot\left[\eta(\nabla\underline{u}+(\nabla\underline{u})^T\right]+F \qquad \nabla\cdot\underline{u}=0 \qquad (1)$$

Eq.(1) is solved for the velocity vector [m/s] and the pressure p [Pa]. The values of ρ and η represent the density [kg/m^3] and the dynamic viscosity [Pa·s]. The fluid flow is considered to be laminar for this particular problem.

Beside the electrical energy, the fuel cells generate heat at the operating points, which determines thermal conditions of the cooling geometry. The governing equation for stationary heat transfer is shown in Eq.(2).

$$\nabla\cdot(-k\nabla T)=Q-\rho\, C_p\underline{u}\cdot\nabla T \qquad (2)$$

It is solved for the variable T. Coefficients k and C_p represent the thermal conductivity [W/m·K] and the specific heat capacity [J/kg·K].

2.3 Boundary Settings

As mentioned above, symmetry conditions are applied to save computational costs because of the complexity of the 3D model geometry. So, only one node of the entire metallic bipolar plate is taken into account due to the geometrical analogy (repeating elements) as depicted in Fig.2.

The velocity and pressure values (table 1) at the inlet and outlet are assigned to the cooling medium for the incompressible Navier-Stokes application mode (application mode constraints).

Table 1: Boundary conditions for the Navier-Stokes application mode

Inlet velocity	1.1 [m/s]
Outlet pressure	101.325 [kPa]

Additionally the velocity at the inlet is parameterized and the overall effects examined separately.

As for the heat transfer application mode the temperature at the inlet is defined as ambient conditions. Additionally, convective flux is assigned to the outlet boundary. A heat flux boundary condition is used to model the heat transfer from the metallic bipolar plate towards the cooling air. This is realized with a heat transfer coefficient h_{ave} from the material data library of COMSOL Multiphysics® [8]. As for this coefficient, an expression for laminar fluid flow and convection (Eq.(3)) is selected and applied on the active surfaces which can be seen in Fig.3 (highlighted in light red). The mean operating temperature of the PEM fuel cell is used to define the overall temperature level. It is taken into account within the heat transfer application mode.

$$h_{ave} = \frac{3.66 \cdot k}{L} \tag{3}$$

In the above equation, h_{ave} is the heat transfer coefficient [W/m^2·K], k is the thermal conductivity [W/m·K], and L is convective length scale [m]. The material properties are defined by utilizing the library functions. Dependant material properties on simulation variables support the multiphysical characteristics of this study.

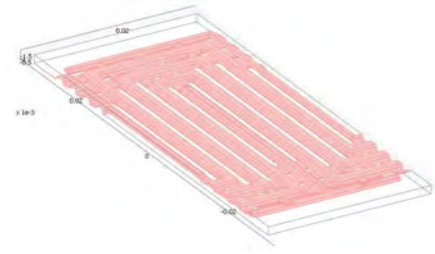

Figure 3. Active surfaces used for the heat flux boundary condition.

2.4 Meshing and Solver Settings

Meshing is performed carefully for this complex 3D model geometry considering the computing capacity. Increasing the number of mesh elements reduces the dependency of the results from the meshing properties. Meshing of a selected geometry can be seen in Fig.4 (312,526 degrees of freedom, and a mesh quality of 0.0622).

Figure 4. Mesh model of one selected 3D model geometry.

The solver is selected regarding the number of degrees of freedom and the applied physical phenomena. As a consequence, a segregated solver is chosen to solve for two individual groups. The variables of Navier-Stokes and general heat transfer application modes are assigned to PARDISO and SPOOLES solvers respectively. P2-P1 and quadratic element types are selected for Navier-Stokes and heat transfer application modes. The solver settings, mesh size and the number of degrees of freedom are kept the same (respectively very close to each other) for all simulations in order to be able to compare all the cooling channel concepts in a proper way.

3. Results

The simulation results of the first model indicate poor cooling characteristics as shown in Fig.5. It is seen that the narrow channels prevent cooling medium to flow inside the channels. It causes badly cooled surfaces and affects the cooling performance directly. To get a smooth temperature profile and a better cooling performance the channel geometry is optimized with the help of the simulation results. The free flow of the cooling medium into the channels affects significantly the entire temperature distribution.

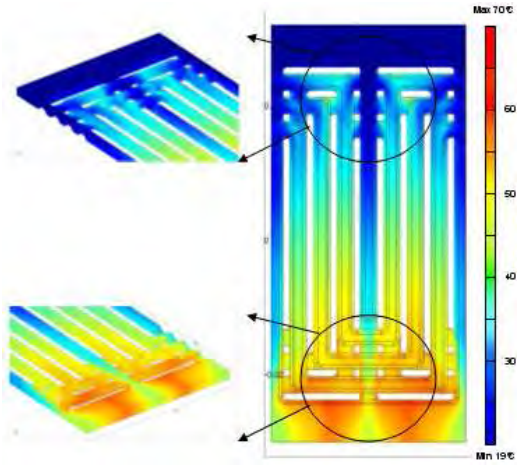

Figure 5. Temperature [°C] distribution of the first design.

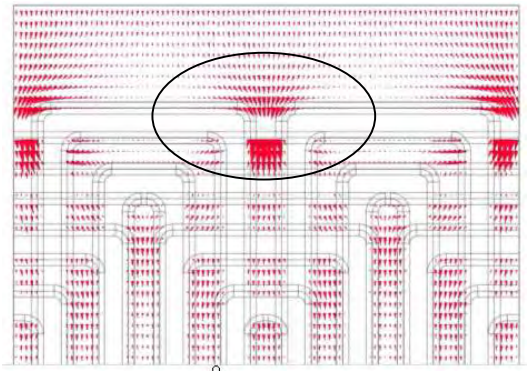

Figure 6. Velocity field arrows for the first design.

The velocity field arrows for the first design can be seen in Fig.6. As it can be depicted from this figure, the narrow inlet channels prevent the cooling medium flow through the channels. This behaviour is improved via increasing the number of the inlet channels through the cooling interface and the second design is performed.

The results for the second design can be seen in Fig.7 and Fig.8. The effect of increasing the number of inlet channels from 3 to 5 leads to an increased flow of the cooling medium into the respective channels. The ameliorated flow behaviour can be seen in Fig.8 when directly comparing it with the Fig.6.

A better (more homogeneous) temperature distribution is achieved with the second design as depicted in Fig.7. But the values are still not smooth enough for optimal cooling behavior.

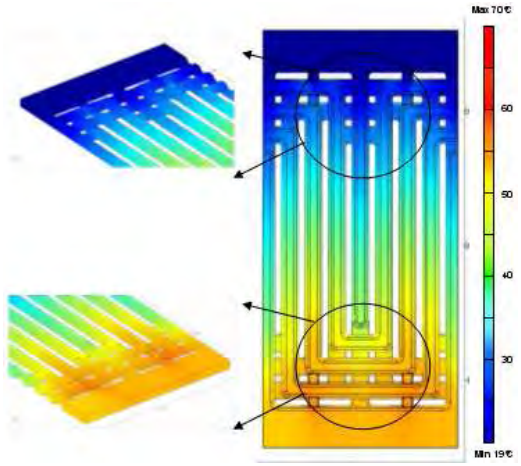

Figure 7. Temperature [°C] distribution of the second design with more inlet channels.

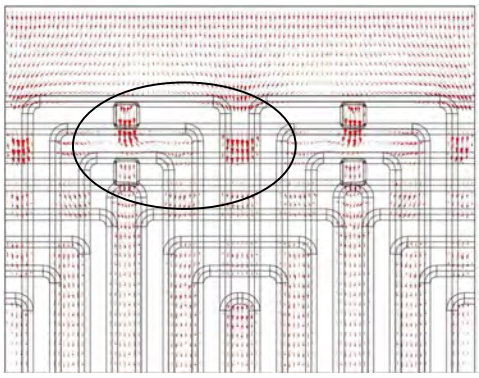

Figure 8. Velocity field arrows for the second design.

With small changes in the height of the cooling channels, a much better thermal distribution is realized.

This geometrical change is performed with the third design. It enhances the air inlet along the inlet channel and assures a better contacting area for the cooling medium.

Additionally, a much smoother temperature distribution is observed (Fig.9).

At the inlet and outlet regions of the cooling medium a more homogenous temperature profile is achieved.

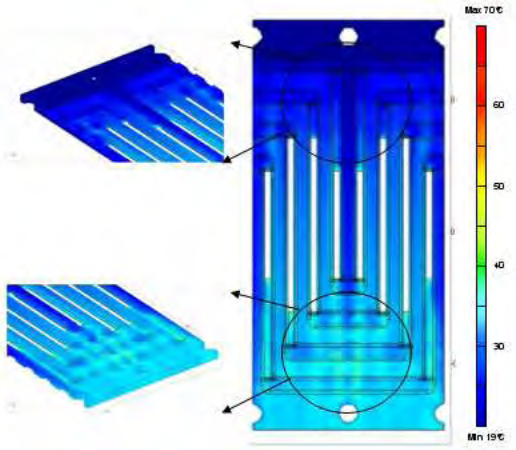

Figure 9. Temperature [°C] distribution of the third design with air inlet along channel.

Changing slightly the height of the cooling channels is the next step for the design optimization. The challenging point is to find optimal cooling channel size without disturbing the gas flow channels of the fuel cell. Hence, a change of the cooling channel geometry yields also changing of the flow field channels which directly affects the cell efficiency. Due to this fact it is prevented to make dramatic changes in the cooling channel size.

Regarding the manufacturing restrictions, the channel size is required to be reduced slightly. Decreasing the height of the channel limits the utilization of straight cooling channel. The results can be seen in Fig.10. This design prevents the cooling medium to flow regularly through the cooling channels which results as bad thermal distribution.

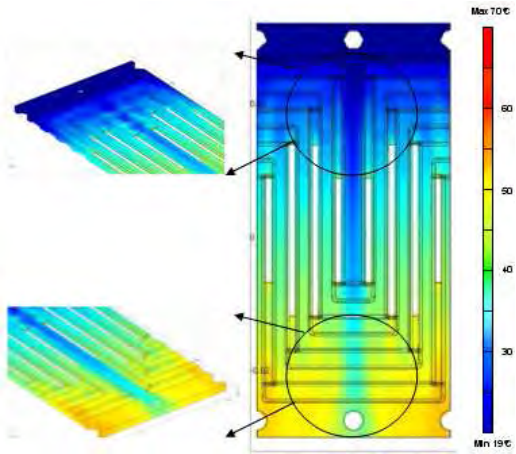

Figure 10. Temperature [°C] distribution of the fourth design with narrower channel depth.

Comparing the third and fourth design in Fig.9 and Fig.10 respectively supplies the final design approach regarding restrictions in the manufacturing process.

Finally, adding another structural bridge at a particular position of the metallic bipolar plate as welding support is evaluated. From the practical point of view, this enables an easier setup of the PEM fuel cell stack and increases the mechanical stability. From the physical point of view it can be depicted from Fig.11 that it facilitates the air flow at the inlet and outlet. This forms the ultimate concept to be produced regarding manufacturing restrictions and simulation results.

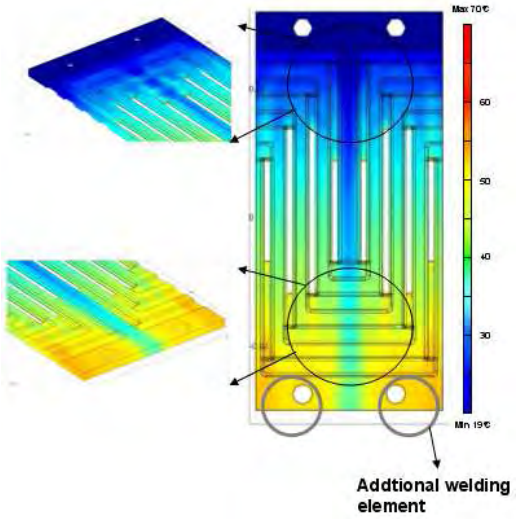

Figure 11. Temperature [°C] distribution of the fifth design with additional welding element.

As mentioned in section 2.3, the inlet velocity is defined as parameter (named V_{in}) and its influence on the physical behaviour evaluated for different values. For this particular study, a parametric segregated solver is chosen and the simulations performed. Selected results can be seen in Fig.12. Increasing the inlet velocity of the cooling medium enhances better thermal distribution. The velocity profile affects directly the convective heat flux and removes more heat from the heated surfaces.

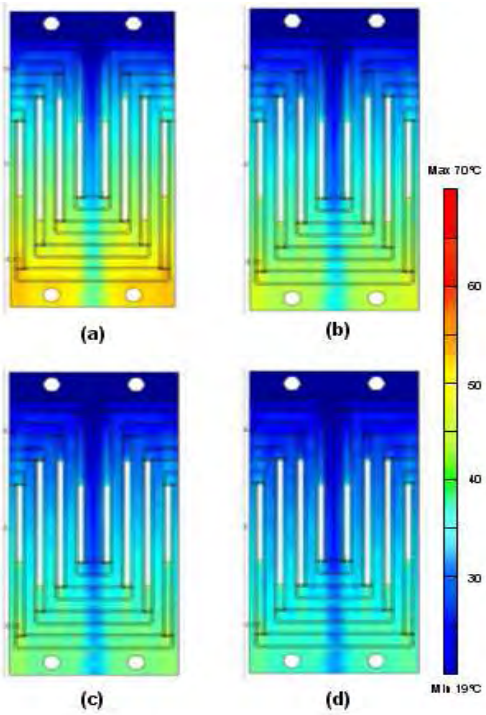

Figure 12. Temperature [°C] distribution of the fifth design with parameterized velocity profile: a) 1.1 [m/s] b) 1.7 [m/s] c) 2.3 [m/s] d) 2.9 [m/s].

Fig.13 and Fig.14 show the boundary integration for both the total heat flux [W] and the temperature [K] for a parameterized inlet velocity. The active boundaries for the heat transfer are selected as seen in Fig.3. It can directly be seen that increasing the inlet velocity affects the cooling performance and results in an increase of the total heat flux as shown in Fig. 13.

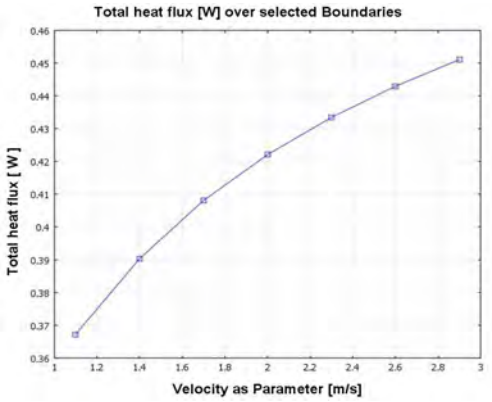

Figure 13. Subdomain integration for total heat flux [W] for different velocity profiles.

The total heat removal from this particular geometry for the inlet velocity 1.1 [m/s] is approx. 0.37 [W] (1.29[W] for one complete cell geometry). In the end, choosing of the peripheral elements of the PEM fuel cell stack for the cooling medium will define the ultimate inlet velocity

It can be depicted from Fig.14 that the mean temperature for the selected boundaries decreases with higher velocity due to the higher convective heat transfer.

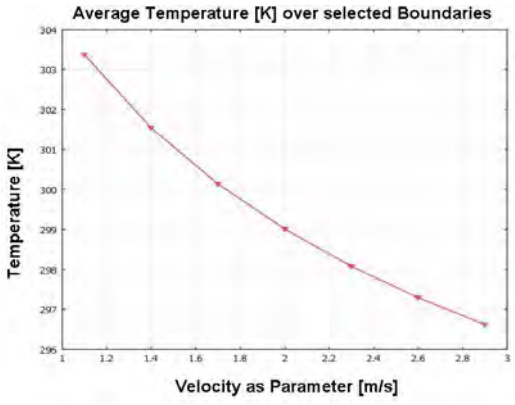

Figure 14. Subdomain integration for the temperature [K] for different velocity profiles.

The fifth concept is finally chosen regarding manufacturing restrictions and simulations. The final plate is seen in Fig.15. Bringing two bipolar plates together builds the cooling channel as shown in Fig.1 and Fig.2. Based on these results, the PEM fuel cell stack is built.

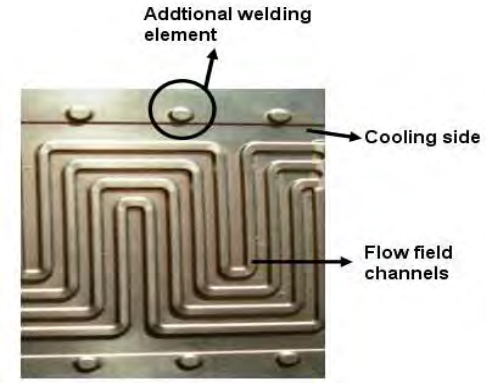

Figure 15. Metallic bipolar plate.

4. Conclusion

The thermal management of a fuel cell system directly affects its performance and

enables the system durability. The control of the thermal distribution is complex compared to the electrical flow due to the non-homogenous characteristics. As already mentioned, both the material properties and the structure of metallic bipolar plates make the cooling issue much more complicated. Herein implementing the cooling structure on the bipolar plate instead of using an additional component limits directly the degree of freedom at the design process but brings many advantages regarding the efficiency and manufacturing process. To be able to realize a proper design concept, the analysis of thermal distribution of metallic bipolar plates is required. The 3D model geometry with all features such as fillets and small faces restricts the simulation model. In order to optimize the cooling channel of metallic bipolar plates, different cooling concepts are simulated and evaluated simultaneously. The simulation results provide better understanding of the cooling phenomena. After producing the prototype and getting first experimental results, the model set-up can be improved regarding thermal constraints. If necessary, the study of the thermal management can be improved by adding electrochemical reactions to the flow field side of the metallic bipolar plate in order to define an improved heat source term.

5. References

1. Wang, J., Derek, O.N., An Investigation on Metallic Bipolar Plate Corrosion in Simulated Anode and Cathode Environments of PEM Fuel Cells using Potential-pH Diagrams, *Int. J. Electrochem. Sci*., **1**, 447-455, (2006)
2. Wind, J., Späh, R., Kaiser, W., Böhm, G., Metallic Bipolar Plates for PEM Fuel Cells, *Journal of Power Source*, **105**, 256-260, (2002)
3. Kreuz, C., PEM-Brennstoffzellen mit Spritzgegossenen Bipolarplatten aus hochgefülltem Graphit-Compound, Universität Duisburg-Essen, Dissertation, (2008)
4. Myung, S.-T., Sakurada, S., Kumagai, M., Yashiro, H., A Promising Alternative to PEMFC Graphite Bipolar Plates: Surface Modified Type 304 Stainless Steel with TiN Nanoparticles and Elastic Styrene Butadiene Rubber Particles, *Fuel Cells 10*, **4**, 545-555, (2010)
5. Berning, T., Djilali, N., Three-dimensional Computational Analysis of Transport Phenomena in a PEM Fuel Cell – A Parametric Study, *Journal of Power Sources*, **124**, 440-452, (2003)
6. Chen, F.C., Gao, Z., Loutfy, R. O., Hecht, M., Analysis of Optimal Heat transfer in a PEM Fuel Cell Cooling Plate, *Fuel Cells*, **3,** 181-185, (2003)
7. COMSOL Heat Transfer Module User's Guide, page: 15, (2008)
8. COMSOL Heat Transfer Module User's Guide, page: 65, (2008)